AERODYNAMIC WAKE INVESTIGATIONS OF HIGH-LIFT TRANSPORT AIRCRAFT WITH DEPLOYED SPOILERS

Ulrich Jung, Christian Breitsamter
Lehrstuhl für Aerodynamik, Technische Universität München,
Boltzmannstr. 15, 85748 Garching, Germany

Keywords: *Aerodynamics, High-Lift, Spoiler, Wake, Transport Aircraft*

Abstract

Commercial Transport Aircraft (CTA) make use of spoilers in the approach phase. In doing so, the aerodynamic wake of the CTA's wing is highly influenced by the deployed spoilers, potentially leading to horizontal tail plane (HTP) buffet. Mean and turbulent flow field quantities downstream of a CTA model's wing are investigated experimentally to evaluate the near field wake. The used detailed half model features slats, aileron and flaps in high-lift approach configuration. Spoiler configurations comprise a baseline configuration with no spoilers deployed, a configuration with outboard conventional spoilers deployed by $\delta = 30°$, and two configurations, with two types of unconventional outboard spoilers. The experiments are performed in Wind Tunnel A at the Institute of Aerodynamics, Technische Universität München. Angles of attack are chosen for each configuration corresponding to a lift coefficient of $C_L = 1.5$. The freestream velocity is set to $V_\infty = 50$ m/s corresponding to a Reynolds number based on wing mean aerodynamic chord of $Re = 1 \times 10^6$. Two stream wise positions are chosen to evaluate the evolution of the wake from near the trailing edge of the wing to the tail of the model. Stereo Particle Image Velocimetry is used to measure the velocity distribution in the wake planes. At selected positions of the planes additional velocity measurements are taken by means of Constant Temperature Hot-Wire Anemometry. These time-resolved measurements serve to conduct a spectral analysis. It is shown that the wake of none of the three investigated spoiler configurations does impose a significant increase of vertical turbulence intensity on the HTP; neither broadband nor narrowband.

Nomenclature

b	= model wing span
c	= wing mean aerodynamic chord
C_L	= lift coefficient, $2L/\rho U_\infty^2 S$
f	= frequency
k	= reduced frequency, $f\,b\,/\,(2U_\infty)$
L	= lift
Re_∞	= freestream Reynolds number based on wing mean aerodynamic chord, $U_\infty c/\nu_\infty$
S	= wing planform
$S_{w'}$	= power spectral density of w'
Tu_z	= vertical turbulence intensity, $\sqrt{\overline{w'^2}}\,/\,U_\infty$
U_∞	= freestream velocity
u, v, w	= axial, lateral and vertical flow velocities
w'	= fluctuation part of w
u^*	= nondimensional axial velocity, u/U_∞
x, y, z	= axial, lateral and vertical coordinate
x^*	= nondimensional axial coordinate, x/b
y^*, z^*	= nondimensional y, z coordinates, $2y/b$, $2z/b$
α	= angle of attack
δ_S	= spoiler deflection angle
ν_∞	= freestream kinematic viscosity
ρ	= air density

Copyright © 2010 by U. Jung and C. Breitsamter. Published by the International Council of the Aeronautical Sciences (ICAS), with permission.

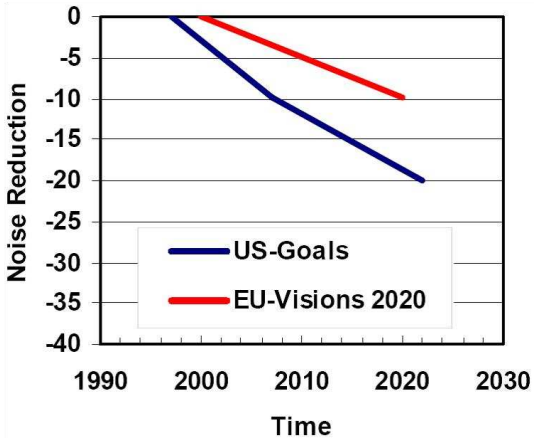

Fig. 1 US and EU-goals for reducing received noise [4]

1 Introduction

Since the 1950s air transport has become a means of mass transportation - its growth is exponential [1]. To avert noise from airport neighbors, a growth in airport noise restrictions for departing and approaching commercial transport aircraft (CTA) is distinctive [2]. The EU Advisory Council for Aeronautical Research in Europe asks in their Vision 2020 [3] for a reduction of noise impact by one half per operation relative to the technology of the year 2000 (Fig. 1). NASA's goals in their Quiet Aircraft Technology Program comprise a reduction of perceived noise impact of future aircraft by one half relative to the technology of the year 1997 within ten years and by three quarters (-20 dB) within 25 years. One has to note, that a reduction by one half corresponds to a reduction of 90% in sound power.

The noise sources of commercial aircraft can be split in two categories: the first category covers all the sources generated by the propulsion unit, the second being the noise sources associated with the airframe. On modern civil transport aircraft airframe and propulsion noise are approximately of the same magnitude during approach and landing [5]. The reduction of the source noise is investigated in recent years by experimental and numerical methods (CAA) [5].

Besides the reduction of source noise, new operational procedures are essential items to meet the aircraft noise requirements. These comprise first and foremost steeper approach paths potentially combined with the continuous descent approach technique. Investigation on this technology's benefit can be found in [6], [7], [8], and [9].

To permit these slow steep approaches, the aerodynamic performance of the approach setting of conventional commercial transport aircraft is not sufficient. Thus, deflection of some kind of spoiler device is required for steep approaches.

This investigation focuses on the near wake of an approaching CTA, which is highly influenced by the deployed spoilers. Turbulences and vortices in the wake can cause issues concerning horizontal tail plane (HTP) buffet as well as hazard to following aircraft flying into the wake. Therefore, mean and turbulent flow field quantities downstream of a CTA models' wing are investigated to evaluate the near field wake with and without deployed spoilers.

The aerodynamic performance related to the longitudinal motion of the CTA half model, which is used in this investigation, were already experimentally evaluated for various spoiler configurations in [12].

Besides the conventional spoilers, one could imagine other types of air brakes; Mertol for example investigated the feasibility of fuselage air brakes in [10]. Flaig et al. postulate a "high-lift system of minimum complexity" [11]. This infers a modified spoiler system of the same dimensions as the conventional spoiler system. The last consideration led the authors to the idea to investigate two unconventional spoiler types with the same basic dimensions as the model's conventional spoilers.

2 Experimental Setup

2.1 Wind Tunnel Model

A model representing the starboard wing and half fuselage is used, designated as the half-model. Basic geometrical model parameters are representative for a modern twinjet CTA. The

Fig. 2 Transport aircraft half-model in WTA

starboard jet engine is modeled by a through flow nacelle. The nacelle is equipped with two engine nacelle strakes modeled by metal sheets with a tapered leading edge. They are attached in flow direction rectangular to the outside of the nacelle and can lead to a reduction in interference drag, increase in C_{Lmax} and L/D at high α, a broader range of high C_L, and less abrupt stall characteristics [13].

Tests are performed for a typical approach high-lift-configuration, consisting of full-span leading edge slats, discontinuous only at the nacelle mount, inboard as well as outboard single slotted fowler flaps and a drooped aileron. The deflection of the high-lift devices is chosen to represent a full-landing configuration. A picture of the half-model installed in Wind Tunnel A (WTA) of the Institute of Aerodynamics of Technische Universität München can be found in Fig. 2.

To reduce the interaction of the wind tunnel floor boundary layer with the aerodynamics of the half-model, it is supported with small clearance directly above an earthed peniche, having the same outline as the fuselage. The gap between fuselage and peniche is closed with a labyrinth seal. Earnshaw et al. show the feasibility to use a half-model with peniche instead of a full-model to receive appropriate results for stall incidence, lift, drag and pitching moment of high lift configurations [14].

The Reynolds number Re_∞ represents the most important dimensionless quantity for viscous flow phenomena to ensure dynamic similarity [15]. For all tests a wind tunnel freestream velocity of $V_\infty = 50$ m/s was chosen, which leads to $Re_\infty \approx 1.0 \times 10^6$ based on wing mean aerodynamic chord. This is at least one order of magnitude lower than in real flying conditions. To achieve realistic aerodynamic values out of the wind tunnel tests, the transition of the boundary layer from laminar to turbulent is tripped by strips at positions, where transition is anticipated for the real aircraft. Transition strips are used around the leading edge of the nacelles as well as at the nose of the fuselage. The pressure distribution on the wing with slats deployed provokes a natural transition at or near the leading edge that makes an artificial transition unnecessary on the wing [16].

2.2 Spoiler Setup

The design of multi-element airfoil systems ordinarily involves the modification of a cruise airfoil in order to provide high lift for takeoff and landing. Extremely rigid constraints relating to mechanical retractability serve to limit the aerodynamically design in terms of both the shape and orientation of the airfoil elements. Considering these limits, it is self evident to investigate spoiler concepts fitting into the existing high lift design. More precisely, all herein investigated spoiler types only affect the wing shroud geometry already used by the conventional spoiler system. The elements studied comprise the planform of the two most outboard located conventional spoilers. These two spoilers were integrated in a single model part. It constrains the investigations to simulate a simultaneous deflection of both control surfaces. This applies also to the alternative spoiler concepts. The investigated air brake concepts are characterized by the following details:

a) *Baseline configuration (BL):* The high-lift configuration with no air brake deflection serves as baseline. Deflected are

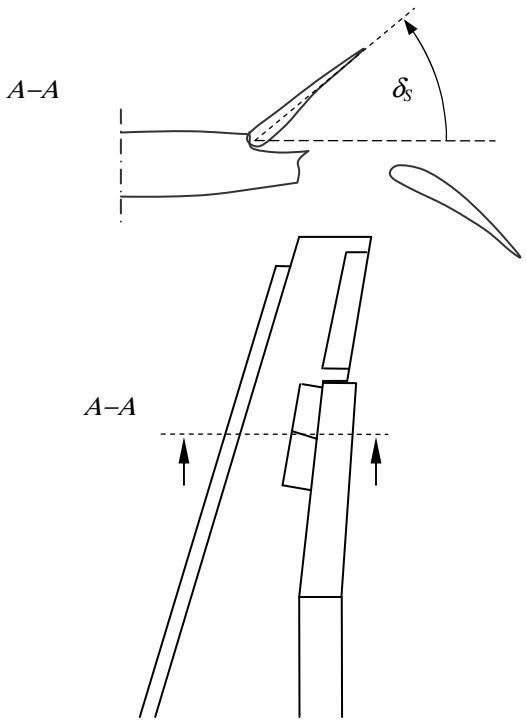

Fig. 3 Schematic view and definition of deflection angle δ_S of conventional spoiler (CS).

leading edge slats, inboard as well as outboard single slotted fowler flaps and the aileron. The deflection of the high-lift devices is chosen to represent a full-landing configuration.

b) *Conventional spoiler (CS)*: This type of air brake can be found on any modern transport aircraft. A segment of the wing's shroud is hereby deflected upwards, leaving a wide opening between the rear end of the wing and the flap. In Fig. 3 a thumbsketch gives an overview of the CS configuration. To get an impression of the model parts, Fig. 4 shows a detailed view of the half-model's wing in the vicinity of the spoiler.

c) *Unconventional spoiler 1 (U1)*: This configuration comprises a novel spoiler of the same basic dimensions and at the same position as CS.

d) *Unconventional spoiler 2 (U2)*: This is a modified version of U1.

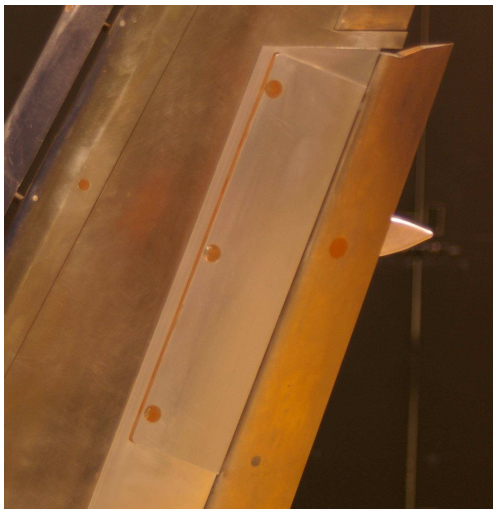

Fig. 4 Detail view of the wing including the conventional spoiler (CS) model.

All air brake configurations are investigated for a fixed spoiler deflection of $\delta_S = 30°$. A positive deflection is defined as an upward rotation of the spoiler, as illustrated in Fig. 3. The angle of attack is chosen for each configuration corresponding to a lift coefficient of $C_L = 1.5$.

2.3 Test Facility

All tests are conducted at continuous low-speed Wind Tunnel A at the Institute of Aerodynamics, Technische Universität München (WTA). The facility features a closed circuit and an open test section. General operating data of WTA can be found in Table 1.

Table 1 Operating data of WTA [17]

Maximum velocity	$V_\infty = 65$ m/s
Cross-section	1.80m × 2.40 m
Turbulence intensity	$Tu_{x,y,z} < 0.4\%$
Deviation of flow direction	$\Delta\alpha, \Delta\beta < 0.25°$
Deviation of static pressure	$\Delta p/q_\infty \leq 0.4\%$
Temporal deviation of freestream velocity	$\Delta V_\infty \leq 0.67\%$
Spatial deviation of freestream velocity	$\Delta V_\infty \leq 0.67\%$

2.4 Measurement System

Two methods are used to investigate the near wake of the half-model: Stereo Particle Image Velocimetry (PIV) and Constant Temperature Hot-Wire Anemometry (HWA).

By means of the used PIV-system one has the ability to obtain the distribution of all three

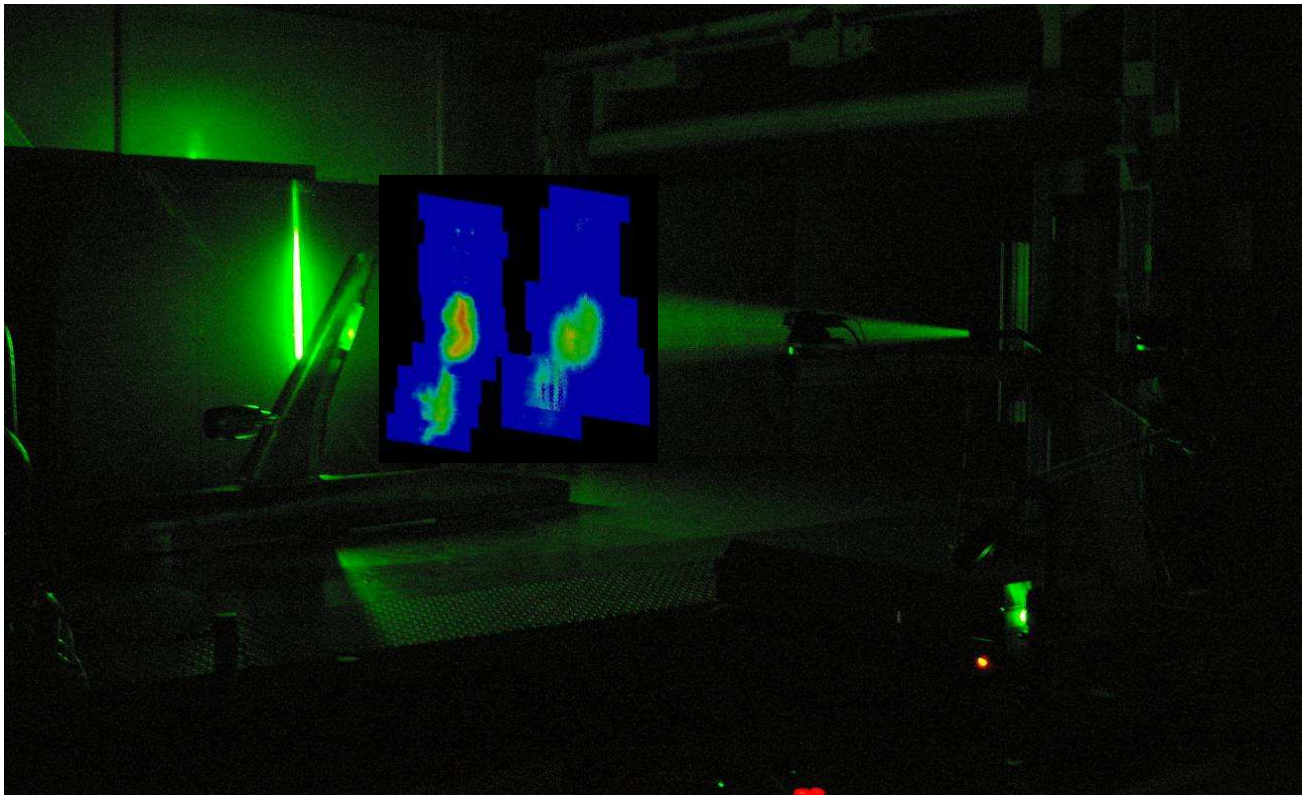

Fig. 5 PIV measurement in progress at WTA. Tu_x in x1 and x2 is visualized in false color representation.

instantaneous velocity components at once for a plane, which is perpendicular to the inflow velocity. The sampling rate of the PIV measurements is $f = 5$ Hz, where 388 samples are recorded per measurement. From this data both the mean velocity components as well as the root mean square velocities can be obtained with a high spatial resolution. A picture of the system in action can be found in Fig. 5. Herein, the laser system unit is on the right hand side. It produces a vertically expanded green laser sheet, which is directed to the left crossing the wake of the half-model's wing. Seeding particles are injected into the air flow. The particle's positions in this laser sheet are recorded by two cameras located upstream and downstream of the measurement plane laterally to the model. By means of cross correlation based on Fast Fourier Transformation, the velocity distribution in the wake plane can then be computed. In Fig. 5, the axial turbulence intensity Tu_x is visualized in false color to represent the two investigated wake planes.

Besides PIV, Constant Temperature Hot-Wire Anemometry (HWA) with a two-wire probe is utilized to examine the instantaneous

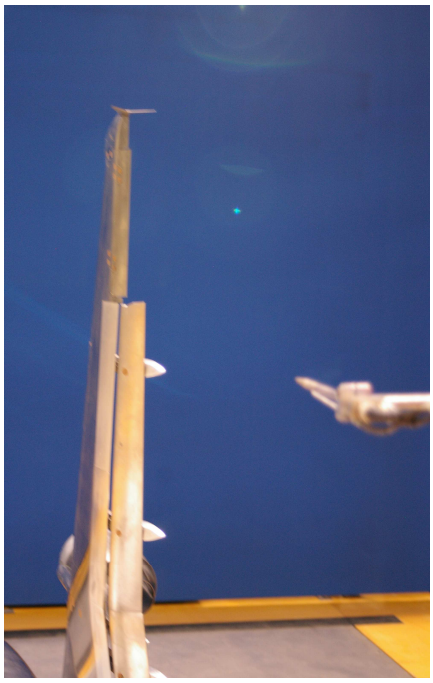

Fig. 6 Hot wire probe traversed in model wake

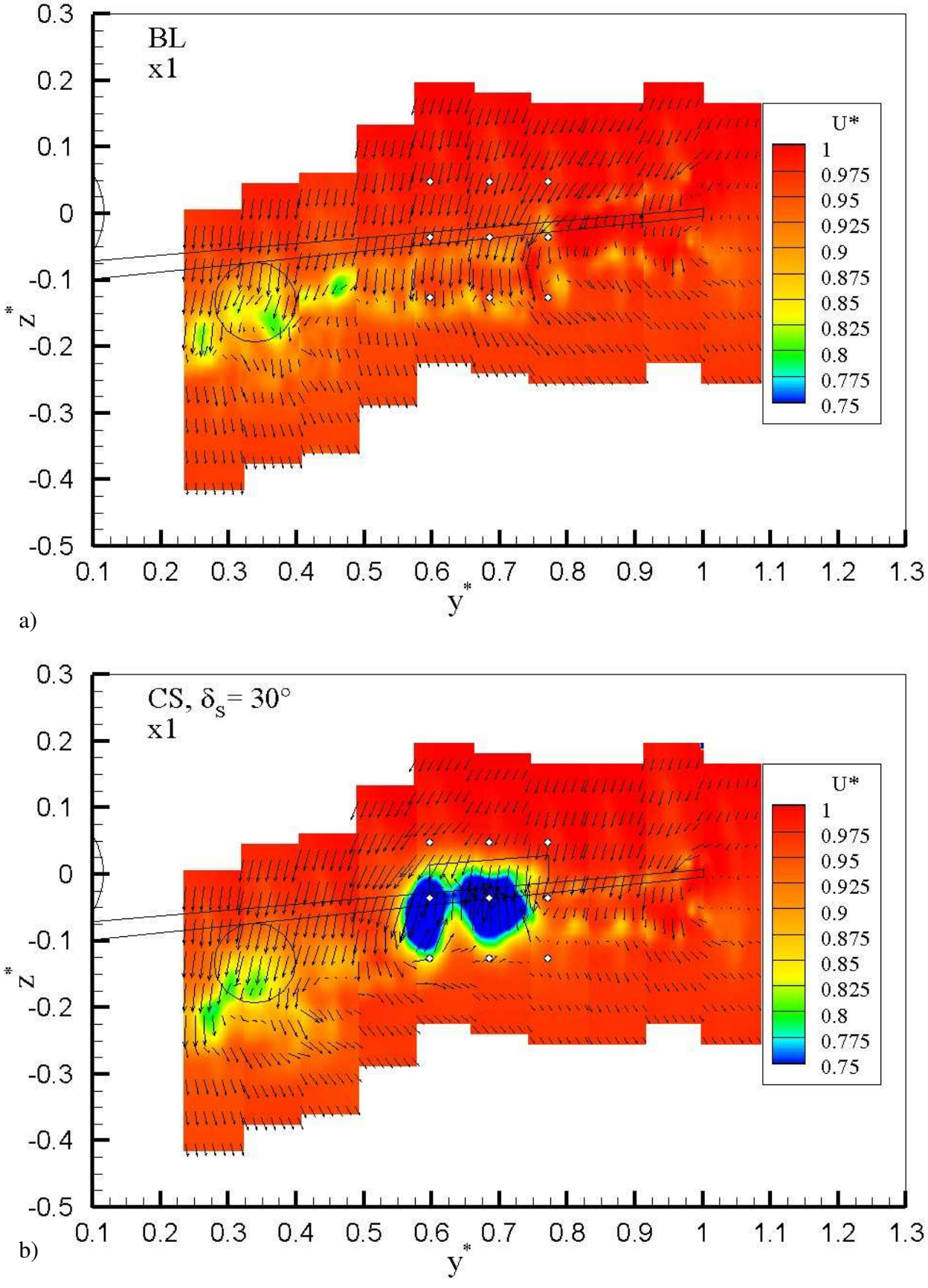

Fig. 7 Velocity distribution in plane x1. a) BL, b) CS

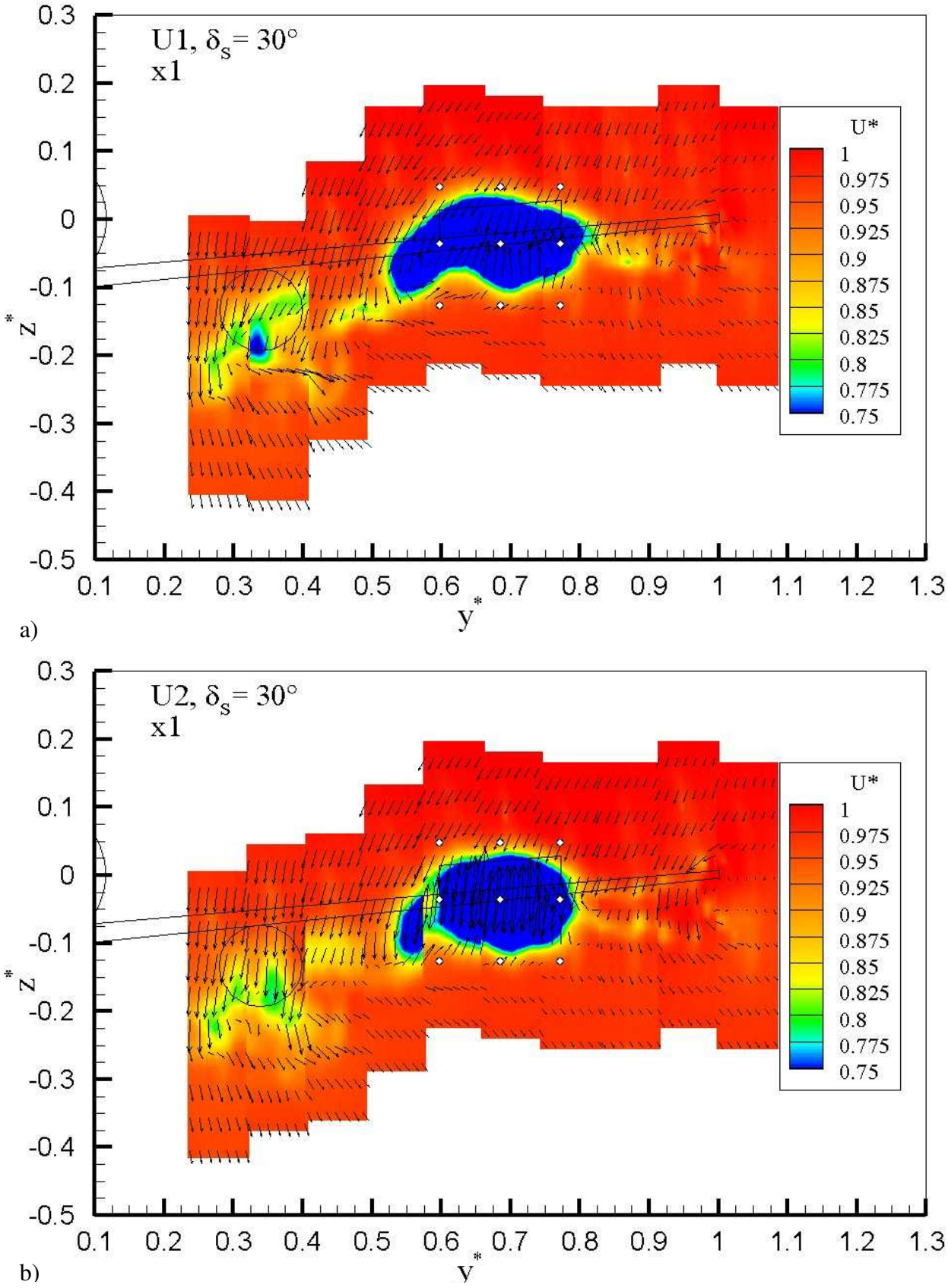

Fig. 8 Velocity distribution in plane x1. a) U1, b) U2

velocity components at selected positions with a high sampling rate of $f = 3000$ Hz. Anemometer output voltages are low pass filtered at 1000 Hz and digitized with 16 bit precision. The measured time is 6.4 s corresponding to 19200 values per hot-wire voltage per measurement station. These measurements serve to conduct a spectral analysis delivering possible dominant frequencies related to respective configurations. The HWA test setup is illustrated in Fig. 6.

2.5 Test Parameters

All measurements are conducted in two planes in the near wake of the half-model's wing. The planes are perpendicular to the inflow velocity vector. The coordinate system is related to the Wing Reference Point (WRP) namely the most outboard position of the wing's trailing edge: $x_{WRP}/b = 0$, $y_{WRP}/(b/2) = 1$, and $z_{WRP}/(b/2) = 0$.

Plane 1 (x1) is defined to be located at $x_1/b = 0.12$. It represents the near field wake of the wing. Plane 2 (x2) is chosen to represent the position of the leading edge of the CTA's HTP, which is not included in the wind tunnel model, and is positioned at $x_2/b = 0.92$.

3. Results

Velocity distributions as well as turbulence intensities of the investigated configurations obtained from the PIV measurements are dicussed in this section. Power spectral densities as function of reduced frequency from the HWA measurements are analyzed for one selected position representing the HTP's tip.

3.1 Velocity Field in Near Wake

Fig. 7a and 7b show the velocity field in plane x1 obtained by PIV for the BL and CS configurations; Fig. 8a and 8b shows it for the U1 and U2 configurations, respectively. The silhouette of the half-model's fuselage, wing, engine nacelle and spoiler is sketched into the pictures to facilitate the attribution of detected flow phenomena to geometrical details of the half-model. The small circles filled with white color in these pictures represent the positions in the plane, for which HWA-measurements were carried out. The positions were chosen to resolve the immediate wake region of the spoiler in this plane.

It is not possible to get the velocity field of the complete wing wake by PIV at once, but only sequentially for rectangular sectors due to the measurement window size of the PIV system. Thus, the PIV laser and camera system is traversed to get ten overlapping sectors in span direction and thereby covering a large wake area reaching from $y^* \approx 0.25$ to $y^* \approx 1.1$. The vertical position of each sector is chosen to incorporate the axial velocity deficit region of the wing wake in the center of the plane. The presented results were not interpolated; the borders of the sectors are not corrected. This sometimes leads to comparatively harsh value intersection from a sector to the next, observed for example in Fig. 8b between sector four and five counted from inboard to outboard.

Analyzing the axial velocity u^* of BL, one can identify the main deficit area is concentrated inboard between $y^* = 0.25$ and $y^* = 0.5$. This is due to the inboard flap and the nacelle positioned upstream of this area. Ranging between $y^* = 0.5$ and $y^* \approx 0.8$, u^*-deficit spots are ordered in two horizontal streaks at $z^* \approx -0.15$ and $z^* \approx -0.08$. Further outboard the streaks are not so clear any more and no more ordered in clear lines, but still observable ranging outboard to $y^* \approx 1$. The crossflow velocity distribution indicated in the figures by arrows shows the downwash in the complete wake plane superposed by vortical structures. These vortices arise at the trailing edge of the wing, where a gradient in the spanwise aerodynamic load distribution is present.

Compared to this, the velocity distribution of CS shows clear differences to BL between $y^* \approx 0.4$ and $y^* \approx 0.75$. Within this interval, two large and strong velocity deficit spots are present. These spots are connected only by a narrow intersection and originate from the deployed spoiler. This spoiler wake region is even more pronounced for both U1 and U2 configurations (Fig. 8a and 8b). For U1, the structure with a large axial velocity deficit ($u^* < 0.75$) is much wider and also no more separated into two spots, but concentrated in one spot with a kidney-like shape. The lateral extension of this

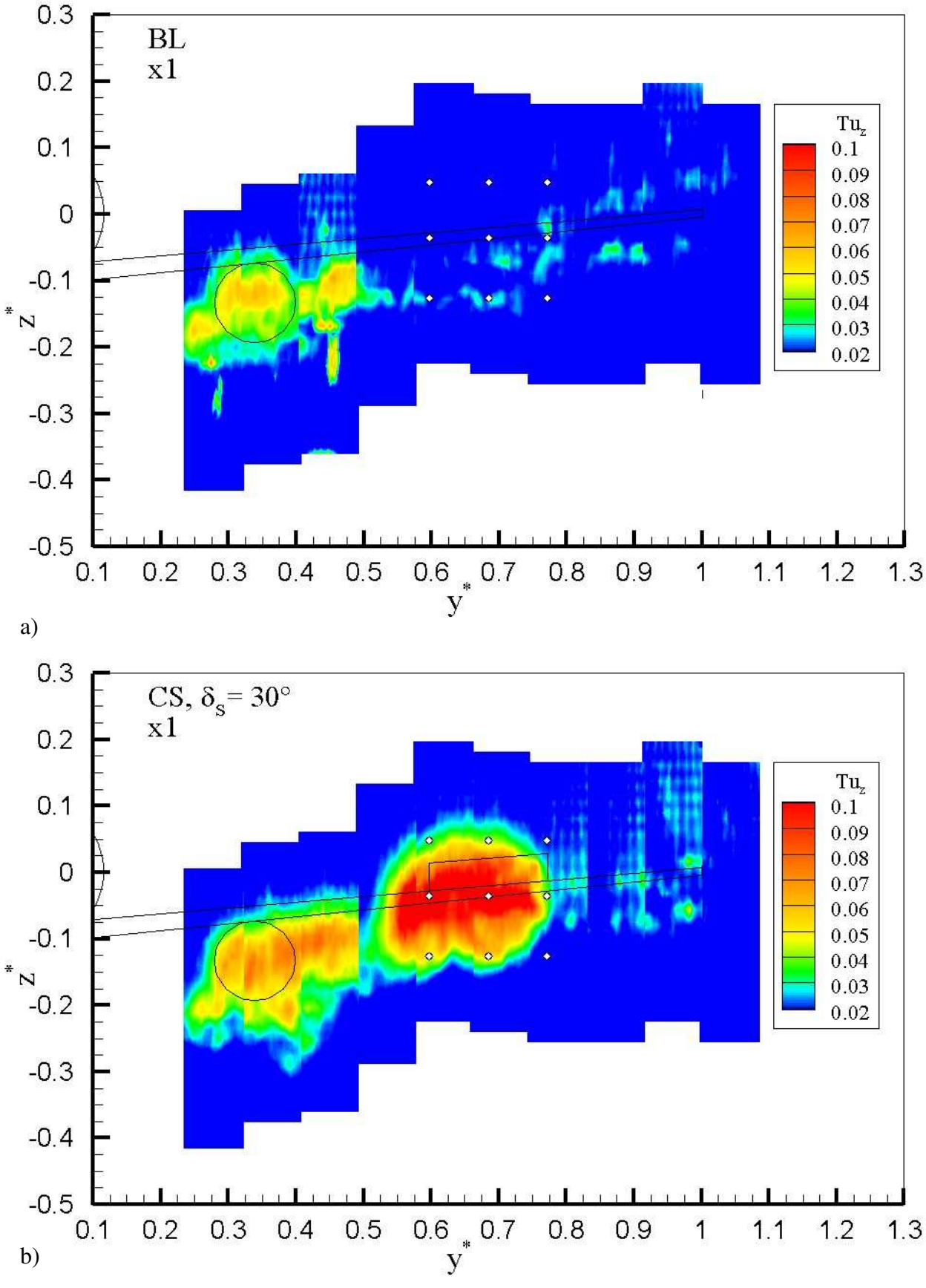

Fig. 9 Vertical turbulence intensity distribution in plane x1. a) BL, b) C1

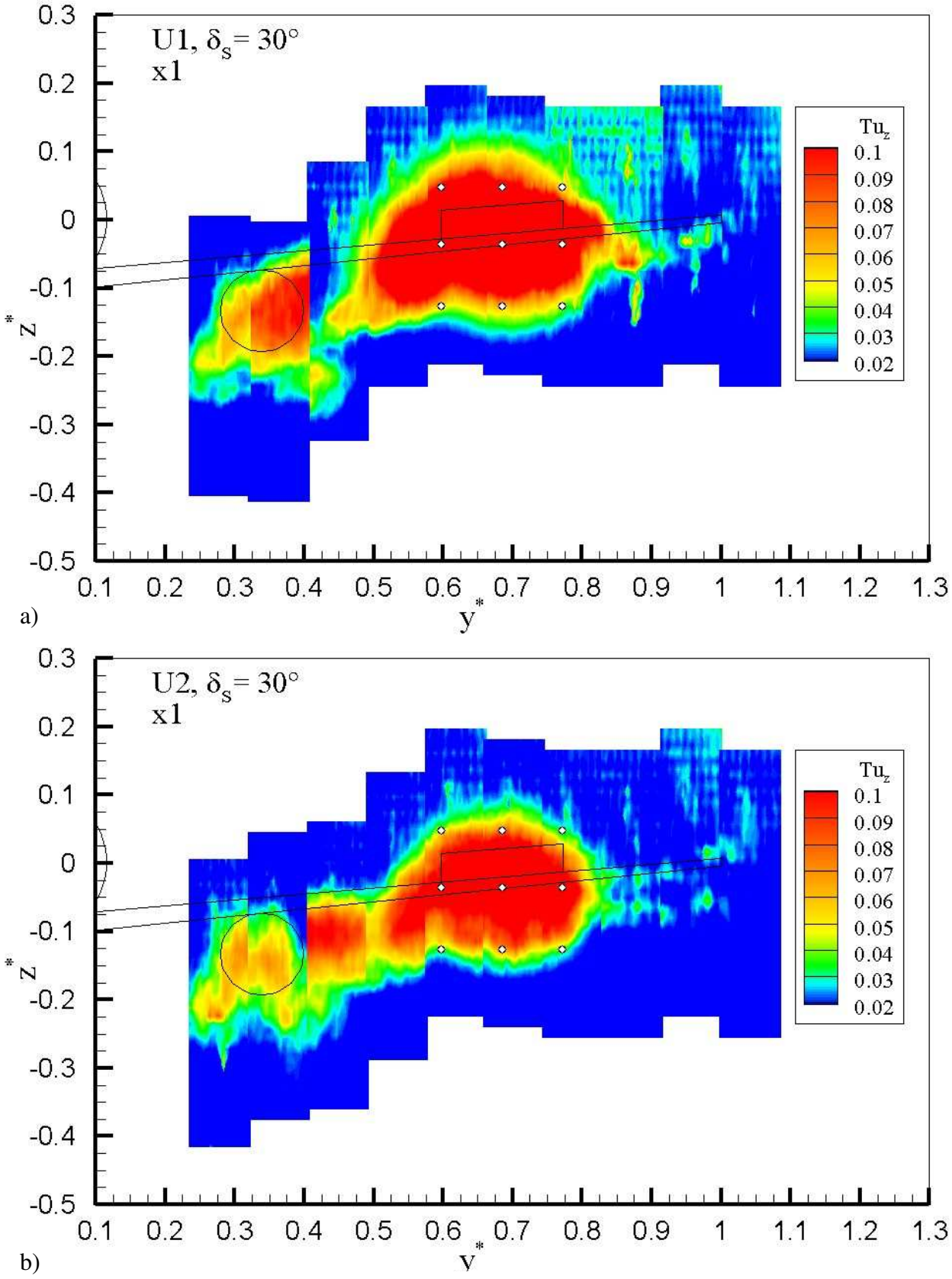

Fig. 10 Vertical turbulence intensity distribution in plane x1. a) U1, b) U2

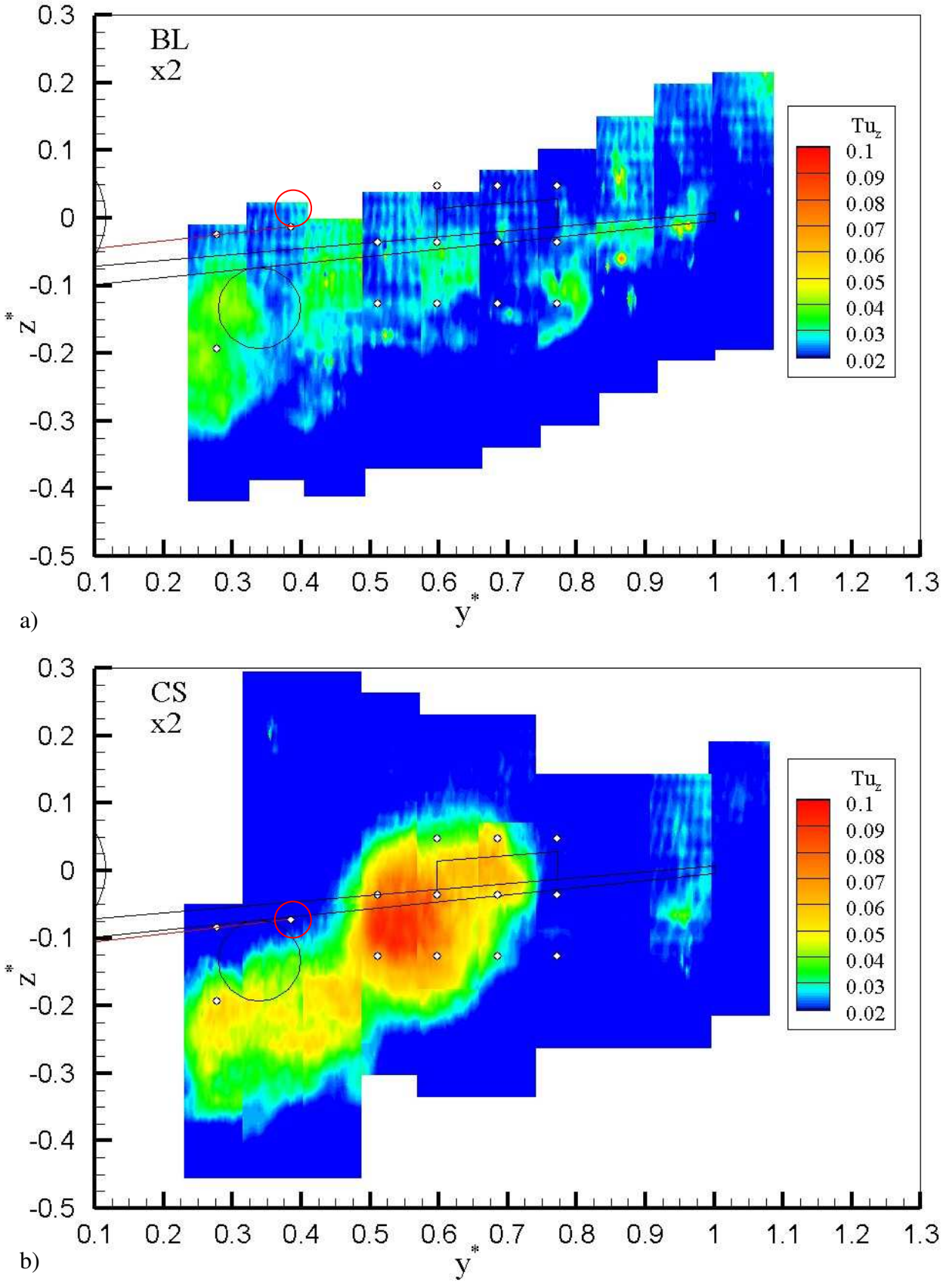

Fig. 11 Vertical turbulence intensity distribution in plane x2. a) BL, b) C1

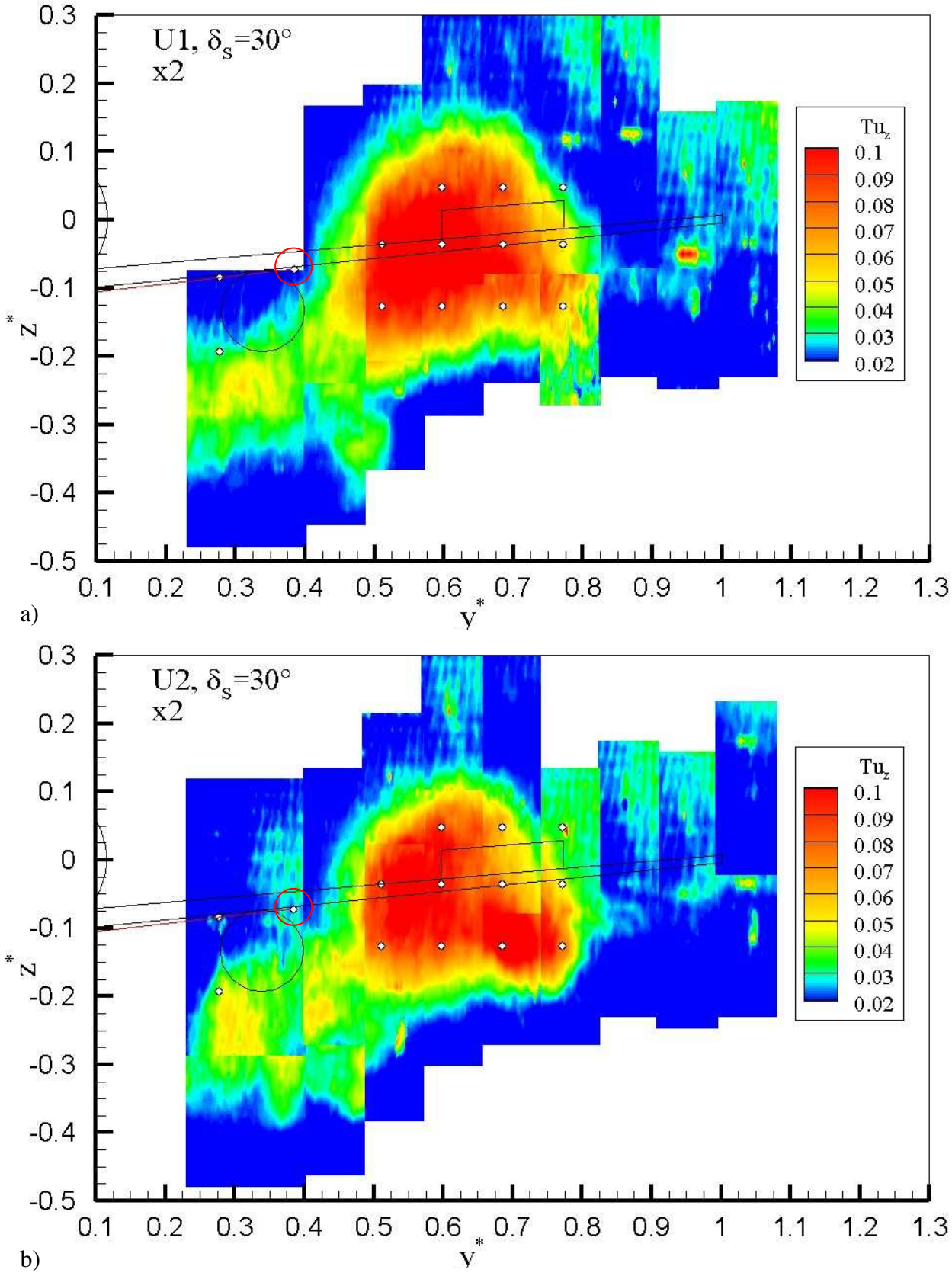

Fig. 12 Vertical turbulence intensity distribution in plane x2. a) U1, b) U2

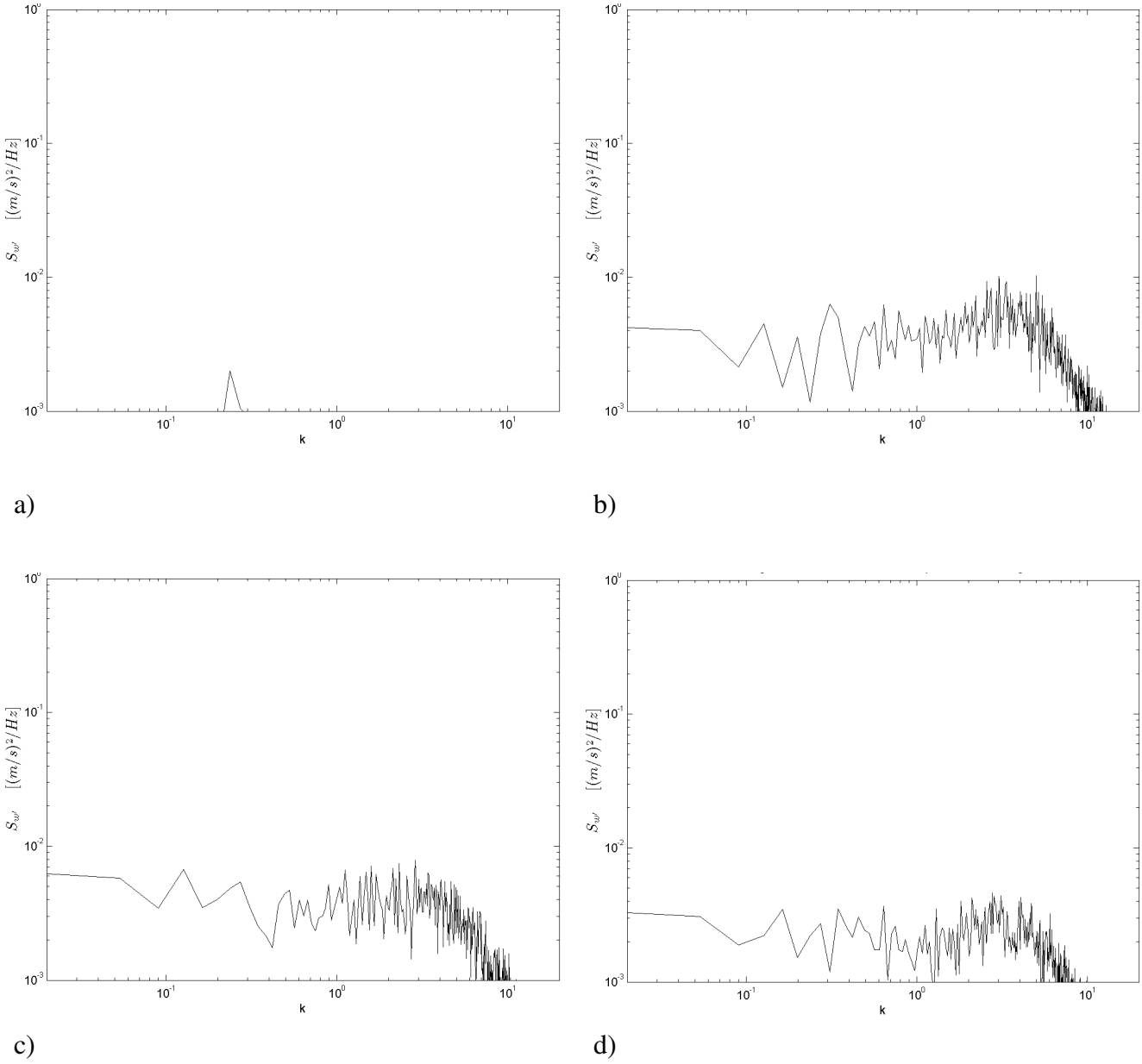

Fig. 13 Comparison of power spectral densities of the vertical velocity fluctuations in plane x2 at in Figs. 11 and 12 marked measurement positions. a) BL, b) CS, c) U1, d) U2

velocity spot has nearly the same size for U2, but an elliptic shape.

3.2 Vertical Turbulence in Near Wake

Figure 9 and Fig. 10 show the vertical turbulence intensity distributions, Tu_z, in plane x1 for all investigated configurations. Figure 11 and Fig. 12 show it in the further downstream located plane x2, which represents the position where the HTP's leading edge is located. Tu_z is accountable for excitation of the HTP, leading potentially to HTP buffet.

All Tu_z-distributions show some scatter of regularly located spots in the low turbulence areas. This is due to a low number of sample points. Nevertheless, the shapes of the high intensity turbulence areas are clearly observable. For all configurations, one distinct high Tu_z structure is observable inboard in plane x1 (Figs. 9 and 10), which is related to the nacelle upstream. The three spoiler configurations feature a second high Tu_z structure related to the

spoilers. For this second structure, significantly larger high Tu_z areas are found for both unconventional spoiler configurations U1 and U2 compared to CS in both planes x1 and x2. Whilst in plane x1, the high turbulence areas of U1 and U2 are elongated in both vertical and lateral dimensions compared to the area of CS, this is different in plane x2: Here, lateral extensions of these high turbulence areas are comparable to the CS configuration, but the areas are vertically more elongated compared to the area of CS and have a different shape.

For all three cases, the area of high turbulence $Tu_z \geq 0.1$ is limited to lateral positions outboard of the HTP's tip. This leads to the conclusion that none of the three spoiler configurations pose danger relating HTP buffet for the investigated zero side slip flow conditions. To further strengthen this conclusion the HWA data are discussed in the following section.

3.3 Spectral Analysis in Near Wake

The white color filled circles in Figs. 11 and 12 represent the positions where HWA-measurements were carried out in the cross flow plane x2. The positions were chosen to resolve the immediate wake region of the spoiler as well as two positions along the span of the HTP. One of these two represents the tip of the HTP - marked by a red circle in Figs. 11 and 12. Exclusively, the HWA results for these HTP tip positions are discussed here. It should be noted that the vertical positions of the measurement points along the HTP's span vary per configuration due to the fact that α is adjusted for each configuration to maintain $C_L = 1.5$.

To analyze the HWA data, a Fast Fourier Transformation was carried out to obtain the power spectral density S as function of reduced frequency k. Figure 13 shows all four configurations' results for the fluctuations of vertical velocity w'. For the baseline case, $S_{w'}$ is smaller than 10^{-3} for all frequencies except a moderate peak at $k = 2.5 \times 10^{-1}$ with $S_{w'} = 2 \times 10^{-3}$. All three spoiler cases show no significant peak at a specific frequency in the power spectral density analysis, but feature a broad band and moderate $S_{w'}$-distribution in the range from $k = 1 \times 10^{-2}$ to $k = 5$. The maximum $S_{w'}$ is thereby $S_{w'} = 4 \times 10^{-3}$ for U2, $S_{w'} = 7 \times 10^{-3}$ for U1 and $S_{w'} = 1 \times 10^{-2}$ for C1. For higher frequencies $k \geq 2.5 \times 10^{-1}$, $S_{w'}$ degrades monotonously in each case.

4 Conclusions

An experimental investigation is conducted to study effects of different spoiler configurations on the near field wake of a commercial transport aircraft configuration. The unsteadiness in the wake is identified to pose potentially a thread to the horizontal tail by inducing buffet phenomena.

A wind tunnel half-model in full approach setting is successively fitted with three spoiler systems, namely a conventional and two unconventional ones. Additionally, the non-spoiler deflection case is investigated representing the baseline configuration. For each configuration, the angle of attack is adjusted to set the lift coefficient to $C_L = 1.5$.

Two wake planes are investigated by means of Particle Image Velocimetry (PIV), which enables to receive the distribution of all three velocity components. The turbulence intensities can also be derived, though no real time resolution is achieved due to the low sampling rate. For this reason, Hot Wire Anemometry is used to supplement the PIV data with velocity measurements of high sample rates at selected positions. Based on these measurements spectral analyses deliver the power spectral density related to each spoiler configuration.

Based on these investigations, all three investigated outboard spoiler configurations pose no risk of HTP buffet for the no side slip condition investigated here exclusively. This is based on the finding, that the HTP is located inboard of the high turbulence areas identified by the PIV measurements and originating from the spoilers. This is the case despite the fact that the turbulent wake region is significantly larger for both unconventional spoilers, but the enlarged regions extend only in the vertical direction. The HWA measurements confirm this just once more by showing moderate values of vertical velocity power spectral density values for all frequencies and all spoiler configurations, though higher values than for the baselinee.

Thereby, the peak values are even lower for both unconventional spoiler configurations compared to the conventional spoiler configuration.

References

[1] Pompl W. *Luftverkehr*. 5th edition, Springer Verlag, ISBN 3-540-42656-6, 2007.

[2] Boeing Co. *Growth in Airport Noise Restrictions*. http://www.boeing.com/commercial/noise/ restrictions.pdf, Homepage Boeing Co., 2008.

[3] Argüelles P, Bischoff M, Busquin P, Droste B A C, Sir Evans R, et al. *European Aeronautics: A Vision For 2020*. Published by EU Advisory Council for Aeronautical Research in Europe (ACARE), ISBN 92-894-0559-7, Jan 2001.

[4] Dobrzynski W. Almost 40 Years of Airframe Noise Research – What Did We Achieve?. *Proc 14th Aeroacoustics Conference*, Vancouver, 5-7 May 2008.

[5] Bieler H, Fischer M, Emunds R, Sutcliffe M. CAA in Industrial Environment: First Analysis of Noise Sources on a 2D High-Lift Profile at Airbus. *Proc 11th AIAA/CEAS Aeroacoustics Conference (26th AIAA Aeroacoustics Conference)*, 23 - 25 May 2005, Monterey, California, AIAA 2005-2977, 2005.

[6] Clarke J P, Ho N H, Ren L, Brown J A, Elmer K R, Tong K O, and Wat J W. Continuous Descent Approach: Design and Flight Test for Lousiville International Airport. *Journal of Aircraft*, Vol. 41, No. 5, pp 1054–1066, Sep 2004.

[7] Tong K, and Warren A. Development of Continuous Descent Arrival (CDA) Procedures for Dual-Runway Operations at Houston Intercontinental. *AIAA Paper*. 2006-7750, Sep 2006.

[8] Hileman J I, Reynolds T G, de la Rosa Blanco E, Law T R, and Thomas S. Development of Approach Procedures for Silent Aircraft. *Proc 45th AIAA Aerospace Sciences Meeting and Exhibit*, Reno, Nevada, AIAA 2007-451, 2007.

[9] Filippone A. Steep-Descent Maneuver of Transport Aircraft. *Journal of Aircraft*, Vol. 44, No. 5, pp 1728-1739, Sep. –Oct. 2007.

[10] Mertol B A. *An Airbrake Design Methodology for Steep Approaches*. STAB06-M071, 2006.

[11] Flaig A, and Hilbig R. High Lift Design for Large Civil Aircraft. *Proc AGARD Conference*, CP-515, pp 31.1–31.12, Sep 1993.

[12] Jung U, and Breitsamter C. Aerodynamics of Transport Aircraft Spoiler Solutions. *Proc KATnet II,* Bremen, Germany, May 2009.

[13] Wallis T. E., Ellis D. R., Wentz, Jr. W. H. The Use of Small Strakes to Reduce Interference Drag of a Low Wing, Twin Engine Airplane. *Proc 9th Atmospheric Flight Mechanics Conference*, San Diego, CA, Aug 9-11, 1982.

[14] Earnshaw P.B., Green A.R., Hardy B.C., and Jelly A.H. A Study of the Use of Half-Models in High-Lift Wind-Tunnel Testing. *Proc AGARD Conference*, CP-515, pp 20.1-20.9, Sep 1993.

[15] Rae W. H., Pope A. Low-Speed Wind Tunnel Testing. 2nd edition, ISBN 0-471-87402-7, John Wiley & Sons Inc., p 7, 1984.

[16] Haftmann B., Debbeler F.-J., and Gielenf H. Takeoff Drag Prediction for Airbus A300-600 and A310 Compared with Flight Test Results. *Journal of Aircraft*, Vol. 25, No. 12, pp 1088-1096, Dez. 1988.

[17] Wind Tunnel A. http://www.aer.mw.tum.de/windkanal/A.en.php, Homepage: Institute of Aerodynamics - Technische Universität München, 2009.

Contact Author Email Address

ulrich.jung@aer.mw.tum.de
christian.breitsamter@aer.mw.tum.de

Copyright Statement

The authors confirm that they, and/or their company or organization, hold copyright on all of the original material included in this paper. The authors also confirm that they have obtained permission, from the copyright holder of any third party material included in this paper, to publish it as part of their paper. The authors confirm that they give permission, or have obtained permission from the copyright holder of this paper, for the publication and distribution of this paper as part of the ICAS2010 proceedings or as individual off-prints from the proceedings.